to the fiber-type grouping used in the previous studies, which had resulted in neurogenic atrophy of the innervated muscles, indicating that the muscular lesions in the BASE cases might not be associated with a neurogenic disorder. The discrepancy might also be due to the use of different technical protocols in tissue processing—specifically, freezing of sections versus formalin fixing and paraffin embedding of sections.

Although L-type BSE cases have been detected throughout Europe, it remains unclear whether the BSE/JP24 prion is identical to other L-type BSE prions. Although the results of this study may accord with those obtained in studies of cattle intracerebrally inoculated with BASE, further research is required to determine if they truly do so. In conclusion, the results of the detailed immunohistochemical and neuropathologic analysis conducted in this study suggest the failure to identify differences between the first- and second-passaged cattle regarding the variables of survival period, molecular properties of PrP^{res}, and other immunohistochemical or neuropathologic features; this suggests that the BSE/JP24 isolate is a biologically and biochemically stable prion in cattle. The findings of the present study will aid future transmission experiments on different L-type BSE isolates.

Acknowledgements

Expert technical assistance was provided by Junko Endo, Mutsumi Sakurai, Noriko Amagai, Tomoko Murata, Naoko Tabeta, and the animal caretaker.

Declaration of Conflict of Interest

The authors declare that they have no conflicts of interests with respect to their authorship or the publication of this article.

Funding

This work was supported by grants from the other Prion Disease Control Project of the Ministry of Agriculture, Forestry, and Fisheries of Japan and the BSE Research Project of the Ministry of Health, Labor, and Welfare of Japan.

References

1. Béringue V, Bencsik A, Le Dur A, et al. Isolation from cattle of a prion strain distinct from that causing bovine spongiform encephalopathy. *PLoS Pathog.* 2006;**2:**e112.
2. Brown P, McShane LM, Zanusso G, et al. On the question of sporadic or atypical bovine spongiform encephalopathy and Creutzfeldt-Jakob disease. *Emerg Infect Dis.* 2006;**12:** 1816–1821.
3. Buschmann A, Gretzschel A, Biacabe AG, et al. Atypical BSE in Germany—proof of transmissibility and biochemical characterization. *Vet Microbiol.* 2006;**117:**103–116.
4. Capobianco R, Casalone C, Suardi S, et al. Conversion of the BASE prion strain into the BSE strain: the origin of BSE? *PLoS Pathog.* 2007;**3:**e31.
5. Casalone C, Zanusso G, Acutis P, et al. Identification of a second bovine amyloidotic spongiform encephalopathy: molecular similarities with sporadic Creutzfeldt-Jakob disease. *Proc Natl Acad Sci U S A.* 2004;**101:**3065–3070.
6. Fukuda S, Iwamaru Y, Imamura M, et al. Intraspecies transmission of L-type-like bovine spongiform encephalopathy detected in Japan. *Microbiol Immunol.* 2009;**53:**704–707.
7. Hagiwara K, Yamakawa Y, Sato Y, et al. Accumulation of mono-glycosylated form-rich, plaque-forming PrPSc in the second atypical bovine spongiform encephalopathy case in Japan. *Jpn J Infect Dis.* 2007;**60:**305–308.
8. Lombardi G, Casalone C, D'Angelo A, et al. Intraspecies transmission of BASE induces clinical dullness and amyotrophic changes. *PLoS Pathog.* 2008;**4:**e1000075.
9. Masujin K, Shu Y, Yamakawa Y, et al. Biological and biochemical characterization of L-type-like bovine spongiform encephalopathy (BSE) detected in Japanese black beef cattle. *Prion.* 2008;**2:** 123–128.
10. Simmons MM, Harris P, Jeffrey M, et al. BSE in Great Britain: consistency of the neurohistopathological findings in two random annual samples of clinically suspect cases. *Vet Rec.* 1996;**138:** 175–177.

Journal of Virology

Absence of CD14 Delays Progression of Prion Diseases Accompanied by Increased Microglial Activation

Keiko Sakai, Rie Hasebe, Yusuke Takahashi, Chang-Hyun Song, Akio Suzuki, Takeshi Yamasaki and Motohiro Horiuchi

J. Virol. **2013, 87(24):13433. DOI: 10.1128/JVI.02072-13. Published Ahead of Print 2 October 2013.**

JVI Journals.ASM.org

Absence of CD14 Delays Progression of Prion Diseases Accompanied by Increased Microglial Activation

Keiko Sakai, Rie Hasebe, Yusuke Takahashi, Chang-Hyun Song,* Akio Suzuki, Takeshi Yamasaki, Motohiro Horiuchi

Laboratory of Veterinary Hygiene, Graduate School of Veterinary Medicine, Hokkaido University, Kita-ku, Sapporo, Japan

Prion diseases are fatal neurodegenerative disorders characterized by accumulation of PrP^{Sc}, vacuolation of neurons and neuropil, astrocytosis, and microglial activation. Upregulation of gene expressions of innate immunity-related factors, including complement factors and CD14, is observed in the brains of mice infected with prions even in the early stage of infections. When CD14 knockout ($CD14^{-/-}$) mice were infected intracerebrally with the Chandler and Obihiro prion strains, the mice survived longer than wild-type (WT) mice, suggesting that CD14 influences the progression of the prion disease. Immunofluorescence staining that can distinguish normal prion protein from the disease-specific form of prion protein (PrP^{Sc}) revealed that deposition of PrP^{Sc} was delayed in $CD14^{-/-}$ mice compared with WT mice by the middle stage of the infection. Immunohistochemical staining with Iba1, a marker for activated microglia, showed an increased microglial activation in prion-infected $CD14^{-/-}$ mice compared to WT mice. Interestingly, accompanied by the increased microglial activation, anti-inflammatory cytokines interleukin-10 (IL-10) and transforming growth factor β (TGF-β) appeared to be expressed earlier in prion-infected $CD14^{-/-}$ mice. In contrast, IL-1β expression appeared to be reduced in the $CD14^{-/-}$ mice in the early stage of infection. Double immunofluorescence staining demonstrated that CD11b- and Iba1-positive microglia mainly produced the anti-inflammatory cytokines, suggesting anti-inflammatory status of microglia in the $CD14^{-/-}$ mice in the early stage of infection. These results imply that CD14 plays a role in the disease progression by suppressing anti-inflammatory responses in the brain in the early stage of infection.

Prion diseases are fatal neurodegenerative disorders including scrapie in sheep and goats, bovine spongiform encephalopathy in cattle, chronic wasting disease in cervids, and Creutzfeldt-Jakob disease in humans. These diseases are characterized by the deposition of disease-specific prion protein (PrP^{Sc}), vacuolation of neurons and neuropil, and astrocytosis in the central nervous system (CNS). Despite little recruitment of adaptive immune cells into the CNS in prion diseases, microglial activation has been observed close to depositions of PrP^{Sc} before neuronal degeneration occurs (1, 2).

Microglia, the resident macrophages of the CNS, survey the environment under physiological conditions. Microbial infections, injury, and neurodegenerative conditions induce microglial activation, characterized by changes in shape, gene expression, and function including cytokine production, phagocytic activity, and antigen presentation (3, 4). Activated microglia are neurotoxic in that they produce proinflammatory mediators such as interleukin-1β (IL-1β), IL-6, tumor necrosis factor alpha (TNF-α), nitric oxide, and reactive oxygen species (5). Alternatively, activated microglia are neuroprotective in that they block proinflammatory responses and produce anti-inflammatory cytokines IL-10, transforming growth factor β (TGF-β), and neurotrophic factors (6).

Previous studies have suggested the significance of a proinflammatory environment in the CNS in the progression of prion diseases. Schultz et al. demonstrated that IL-1β receptor I-deficient mice delayed the onset of prion diseases with attenuated PrP^{Sc} deposition and astrocytosis (7). A protective role of anti-inflammatory cytokines in prion diseases has also been reported: the incubation time in IL-10-deficient mice was greatly shortened (8). Boche et al. showed that inhibition of TGF-β activity in ME7 prion-infected mice induced severe neuronal inflammation and acute neuronal death (9). Taken together, these facts suggest the necessity for the inflammatory environment in the brains of prion-infected mice to be further elucidated for a better understanding of the mechanism of neurodegeneration in prion diseases.

It is well established that PrP^{Sc} accumulation precedes neurodegeneration and clinical manifestations of prion diseases. To analyze the host reaction in prion infection in the brain, particularly during the early stages after intracerebral inoculation of prions, we compared the gene expression of prion- and mock-infected mouse brains by cDNA microarray analysis from 60 to 90 days postinoculation (dpi) (M. Horiuchi and C.-H. Song, unpublished observations). Focusing on genes that have been reported to be expressed by microglia, we found that several innate-immunity-related genes, including *CD14*, and complement factors were upregulated as described in previous studies (10, 11). CD14, a glycosylphosphatidylinositol (GPI)-anchored protein, is well known as a lipopolysaccharide (LPS) receptor. Although CD14 itself cannot induce cellular signaling because of lack of cytoplasmic domains, binding of pathogen-associated molecular patterns to CD14 clusters transmembrane proteins including Toll-like receptor 2 (TLR2) and TLR4 to induce gene expression of proinflammatory mediators (12, 13). Upregulation of CD14 expression associated with deposits of aggregated proteins has been reported in the brains of mouse models and human patients with neurodegenera-

Received 28 July 2013 Accepted 26 September 2013
Published ahead of print 2 October 2013
Address correspondence to Motohiro Horiuchi, horiuchi@vetmed.hokudai.ac.jp.
* Present address: Chang-Hyun Song, Department of Anatomy and Histology, College of Korean Medicine, Daegu Haany University, Gyeongsan, South Korea.
K.S. and R.H. contributed equally to this work.

doi:10.1128/JVI.02072-13

tive disorders including Alzheimer's disease (AD), Parkinson's disease/dementia with Lewy bodies, and amyotrophic lateral sclerosis (14). A polymorphism in the promoter region of the *CD14* gene that affects the expression of *CD14* has been reported to significantly increase the risk of Parkinson's disease in females (15, 16). Depletion of CD14 in an AD mouse model showed a reduced amyloid β (Aβ) plaque burden with altered microglial activation (17). These findings suggest the involvement of CD14 in the pathogenesis of neurodegenerative disorders.

In the present study, we examined if CD14 influences the neuropathology and neuroinflammatory conditions in prion diseases. When CD14 knockout ($CD14^{-/-}$) mice were inoculated intracerebrally with Chandler and Obihiro prion strains, the survival time was significantly prolonged compared to that of wild-type (WT) mice, suggesting that CD14 is involved in the progression of the disease. Our data also suggest that an increased microglial activation in $CD14^{-/-}$ mice accompanied by anti-inflammatory cytokine production may contribute to the prolonged survival time of the $CD14^{-/-}$ mice.

MATERIALS AND METHODS

Antibodies. Anti-mouse prion protein (PrP) monoclonal antibodies (MAbs) 31C6 and 132 were prepared as described previously (18). Anti-Iba1 rabbit polyclonal antibodies were purchased from Wako (product no. 019-20001). Anti-glial fibrillary acidic protein (anti-GFAP) rabbit polyclonal antibodies were from Dako (product no. Z033401). Unconjugated and Alexa Fluor 488-conjugated anti-mouse CD11b rat MAb (clone M1/70), anti-mouse CD14 rat MAb (clone Sal 14-2), and anti-mouse F4/80 rat MAb (clone BM8) were from BioLegend. Anti-NeuN mouse MAb (clone A60) was from Millipore. Anti-mouse CD45 rat MAb (clone 13/2.3) was from Funakoshi. Anti-GFAP mouse MAb (clone GF5), anti-IL-10 rat MAb (clone JES5-2A5), anti-mouse CD68 rat MAb (clone FA-11), anti-TGF-β rabbit polyclonal antibodies (product no. 66043), and anti-IL-1β rabbit polyclonal antibodies (product no. 9722) were from Abcam. ECL horseradish peroxidase-labeled anti-mouse IgG was from Amersham Biosciences (product no. NA9310V). All Alexa Fluor-labeled antibodies were from Life Technologies.

Mice and prion inoculation. C57BL/6J mice were purchased from Japan Clea Inc. CD14 knockout ($CD14^{-/-}$) mice of congenic strain B6.129S-$Cd14^{<tm1Frm>}$/J were purchased from Jackson Laboratories and were further maintained by inbreeding. All animal procedures were approved by the Institutional Animal Care and Use Committee of the Graduate School of Veterinary Medicine, Hokkaido University. Six-week-old female WT and $CD14^{-/-}$ mice were inoculated intracerebrally with 20 μl of 2.5% brain homogenates of the Chandler- or Obihiro-infected C57BL/6J mice. The inoculation was carried out whenever the 6-week-old female $CD14^{-/-}$ mice were available. The exact same aliquots of 2.5% brain homogenates were used for each inoculation. At the clinical stage, mice were observed every day, and the clinical endpoint of disease was defined as recumbency with severe emaciation within two consecutive days.

Quantitative RT-PCR. Total RNA was extracted from the thalamus cut at a thickness of the coronal section with 5 mm around the level of bregma −1.82 mm (as indicated in *The Mouse Brain in Stereotaxic Coordinates*, 2nd ed. [19]) using TRIzol reagent (Life Technologies). First-strand cDNA was synthesized from 2 μg of the total RNA using a First-Strand cDNA synthesis kit (Amersham Biosciences) according to the manufacturer's instructions. The amplification reaction mixtures contained template cDNA, 1× predesigned TaqMan Gene Expression Assays for mouse Cd14 (Mm00438094_g1) and for mouse ACTB (catalog no. 4352933E), and 1× TaqMan Fast Universal PCR Master Mix. TaqMan assays were carried out using an ABI 7900HT Fast Real-Time PCR system (Applied Biosystems). The amplification profiles were analyzed using a threshold cycle relative quantification method and were normalized with the expression of mouse ACTB gene as described previously (20).

Bioassay. Brain homogenates from 2 mice at each time point were prepared in sterile phosphate-buffered saline (PBS) to 1% (wt/vol). Twenty microliters of brain homogenates were inoculated intracerebrally into 6-week-old Tga20 mice. To obtain an infectivity-incubation time standard curve, 10-fold serial diluted brain homogenates used as the inocula of the Chandler and Obihiro strains were also injected into Tga 20 mice. The 50% lethal doses (LD_{50}) of the original 10% homogenates were estimated to be $10^{9.3}$ and $10^{9.5}$ LD_{50}/g brain tissue for the Chandler and Obihiro strains, respectively. In the Chandler infection, the standard curve for the incubation periods (χ) was fitted by the approximations of concentrations of original brain homogenates (y), determined as follows: $y = e^{23.026-0.425\chi}$ for the periods of up to 68 days, and $y = e^{16.118-0.332\chi}$ for the periods after 69 days. In the Obihiro infection, the approximation was $y = e^{20.723-0.263\chi}$ for the periods of up to107 days and $y = e^{7.092-0.129\chi}$ for the periods after 108 days.

PrP-res detection by immunoblotting. For protease-resistant prion protein (PrP-res) detection, at 60, 90, and 120 dpi and at the terminal stage of the disease, brains were harvested and were homogenized in sterile PBS to prepare 10% (wt/vol) brain homogenates. The homogenates were treated with proteinase K (PK) and were subjected to SDS-PAGE and immunoblotting as described previously (20).

PrP^{Sc}-specific immunofluorescence staining. The PrP^{Sc}-specific staining of frozen sections was performed by a method described previously (21) with some modifications. Briefly, the brains were embedded in OCT compound (Sakura Finetek, Japan) and were cut at a thickness of 10 μm. The samples were fixed with 4% paraformaldehyde (PFA) for 10 min at room temperature (rt). The slides were treated with 0.1% Triton X-100 for 10 min at rt and then with 5 M guanidine thiocyanate for 10 min at rt. After washing with PBS, the sections were blocked with 5% fetal bovine serum (FBS) in PBS at 37°C for 30 min. The sections were then incubated with MAb132 at 3 μg/ml at 37°C for 45 min. For the secondary antibody reaction, the sections were incubated with Alexa Fluor 488-labeled anti-mouse IgG $(Fab)'_2$ fragment of goat IgG at rt for 1 h. The samples were counterstained with 4′6-diamidino-2-phenylindole (DAPI), mounted with ProLong Gold antifade reagent (Invitrogen), and then observed with a laser scanning confocal microscope (LSM) (Carl Zeiss International).

Histopathological analysis. The histopathological analysis was carried out as described previously (22). Briefly, brains were harvested at 90 and 120 dpi and at the terminal stage of the disease and fixed with 10% phosphate-buffered formalin. The brains were embedded in paraffin and cut at the level of bregma −1.82 mm. The samples were stained with hematoxylin and eosin (H&E).

Immunohistochemistry. For the antigen retrieval of Iba1 detection in paraffin-embedded tissue, the slides were treated with microwaves at 600 W for 10 min in 0.01 M citrate buffer solution, pH 6.0. After washing with PBS, the slides were blocked with normal goat serum (Nichirei) and incubated overnight with primary antibody diluted at 1:1,000 in normal goat serum at 4°C. The slides were treated with 0.3% hydrogen peroxide in methanol to block endogenous peroxidase activity at rt for 10 min. Biotin-labeled anti-rabbit IgG goat polyclonal antibodies (Nichirei) were incubated for 10 min at rt. Peroxidase-labeled streptavidin (Nichirei) was reacted for 5 min at rt. The immunoreactivity was visualized with Impact DAB (Vector). For quantitative analysis of Iba1-positive microglia, cells with more than 10 μm^2 of Iba1 immunoreactivity were counted by Image J (U.S. National Institutes of Health, Bethesda, MD, USA; http://rsb.info.nih.gov/ij/).

For the immunohistochemistry of the microglial markers and cytokines in frozen tissue, brains were embedded in the OCT compound (Sakura Finetek, Japan) and were cut at a thickness of 10 μm. Sections were fixed with 4% PFA for 10 min at rt. For the antigen retrieval, samples were treated with 0.1% Tween 20 in PBS for 15 min at rt. The slides were blocked with 2% bovine serum albumin for 15 min at rt and incubated overnight with primary antibody at 4°C. Then, slides were incubated with

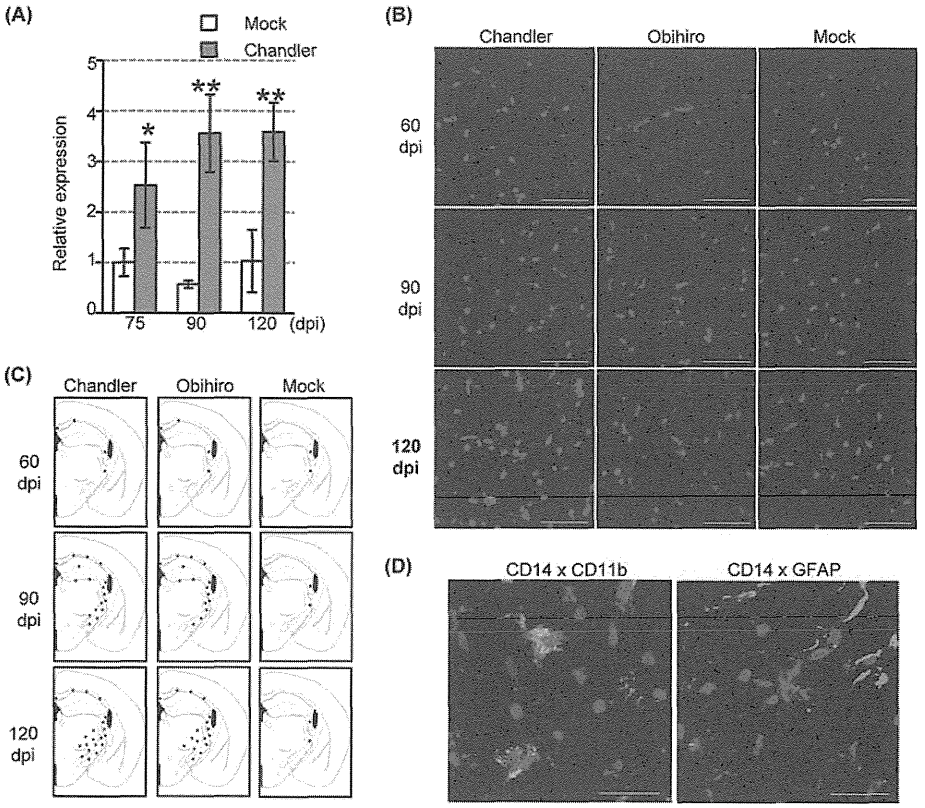

FIG 1 Expression of CD14 in the brains of prion-infected WT mice. (A) Gene expression of *CD14*. Total RNA was extracted from the thalamus of Chandler- and mock-infected WT mice at 75, 90, and 120 dpi and subjected to quantitative RT-PCR. Expression of the *CD14* gene in the thalamus of the mock-infected mice at 75 dpi was defined as 1, and relative expressions are shown. *, $P < 0.05$; **, $P < 0.01$ (Student's *t* test). (B) Immunofluorescence staining of CD14 in the cerebral peduncle. The brains of Chandler-, Obihiro-, and mock-infected mice were harvested at 60, 90, and 120 dpi. Frozen sections at the level of bregma −1.82 mm were subjected to immunofluorescence staining of CD14 (red). Blue, nuclear counterstaining with DAPI. Bars, 50 μm. (C) Summary of the distribution of CD14 in the brains of Chandler-, Obihiro-, and mock-infected mice. Illustrations show the level of bregma −1.82 mm as indicated in *The Mouse Brain in Stereotaxic Coordinates*, 2nd ed. (19). (D) Double immunofluorescence staining of CD14 (green) with CD11b (left, red) or GFAP (right, red). Representative figures from the cerebral peduncles of the Chandler-infected mice at 120 dpi are shown. Blue, nuclei. Bars, 20 μm.

secondary antibodies and DAPI for 1 h at rt. Finally, slides were mounted with ProLong Gold antifade reagent (Invitrogen) and observed with LSM700 (Zeiss). For the detection of CD14, CD45, and CD68, the antibodies were diluted at 1:800. For CD11b, TGF-β, and IL-1β, the antibodies were diluted at 1:200. For IL-10, the antibody was diluted at 1:100. For GFAP and F4/80, the antibodies were diluted at 1:1,000. For secondary antibodies, all Alexa Fluor-labeled antibodies were diluted at 1:1,000.

RESULTS

Expression of CD14 is increased in microglia and accompanied by progression of prion diseases. Previous DNA microarray analyses have suggested that gene expression of *CD14* was upregulated in prion-infected mouse brains in the early stage of infection (10, 11) (M. H. and C.-H. Song, unpublished). To confirm the gene expression of *CD14*, we performed a quantitative RT-PCR (Fig. 1A). The *CD14* gene expression in the thalamus of the Chandler-infected mice was 2.5 ± 0.8, 3.6 ± 0.8, and 3.6 ± 0.6 higher than that in the thalamus of mock-infected mice, at 75, 90, and 120 dpi, respectively, confirming the upregulation of *CD14* expression. We also performed immunofluorescence staining of frozen sections of the Chandler- and Obihiro-infected mice brains to confirm the protein expression of CD14 (Fig. 1B), and CD14-positive cells were most frequently detected in the cerebral peduncle at the observed time points (Fig. 1B). The CD14-positive cells were scattered in corpus callosum, internal capsules, and cerebral peduncles at 60 dpi, spreading more widely in the cerebral peduncles and periventricle areas at 90 dpi, and the spreading had expanded to the thalamus at 120 dpi (Fig. 1B and C). A few CD14-positive cells were also detected in the internal capsules and cerebral peduncles of mock-infected mouse brains, suggesting that these cells may be residents in these areas (Fig. 1C). To confirm the CD14 expression in the microglia, double staining of CD14 with CD11b for microglia and of GFAP for astrocytes was performed (Fig. 1D). Most of the CD14 immunoreactivity was detected in the CD11b-positive microglia, but it was not detected in the GFAP-positive astrocytes.

CD14 influences the progression of prion diseases. To examine the effect of the lack of CD14 on the neuropathogenesis of prion diseases, we inoculated brain homogenates of the Chandler or Obihiro strain-infected mice into $CD14^{-/-}$ mice (Fig. 2). The $CD14^{-/-}$ mice infected either with the Chandler strain or with the Obihiro strain survived longer than the WT mice. The mean survival time of the Chandler strain-infected $CD14^{-/-}$ mice (161.7 ± 3.7 days, $n = 11$) was significantly longer than that of the WT mice (153.8 ± 3.7 days, $n = 12$, $P < 0.01$, Student's *t* test) (Fig. 2A). The mean survival time of the Obihiro strain-infected $CD14^{-/-}$ mice

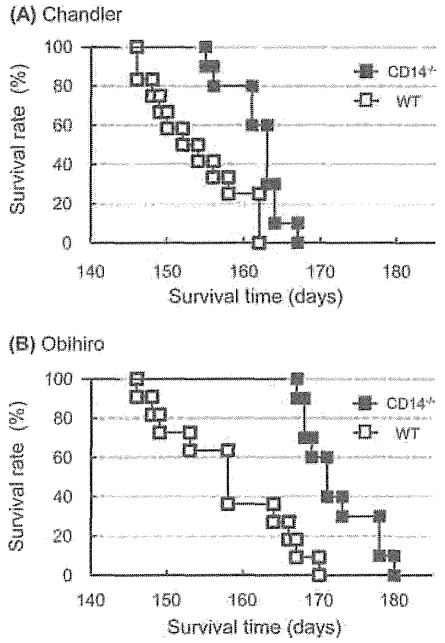

FIG 2 Survival times of WT and CD14$^{-/-}$ mice infected with the Chandler or Obihiro strain. (A) Survival curves of the Chandler-infected WT and CD14$^{-/-}$ mice. (B) Survival curves of the Obihiro-infected WT and CD14$^{-/-}$ mice.

(172.3 ± 4.8 days, $n = 10$) was also significantly longer than that of WT mice (157.9 ± 7.8 days, $n = 11$, $P < 0.01$, Student's t test) (Fig. 2B). These results suggest that the lack of CD14 decelerates the progression of the disease.

To determine if knockout of CD14 influences the accumulation of PrP^{Sc}, we analyzed the PrP-res accumulation in the brains by immunoblotting (Fig. 3A and B). The intensity of the PrP^{Sc} signals in the brains of CD14$^{-/-}$ mice infected with either the Chandler or the Obihiro strain was slightly reduced at 90 and 120 dpi and became comparable to that seen in the WT mice at the terminal stage.

We have reported that MAb132, recognizing amino acids 119 to 127 of mouse PrP, in combination with pretreatment of cells with 5 M guanidine thiocyanate, is useful for the PrP^{Sc}-specific immunofluorescence staining of prion-infected cell cultures (21). It is well established that PrP^{Sc} includes protease-sensitive and protease-resistant PrP^{Sc} (23, 24). The protease-sensitive PrP^{Sc} that cannot be detected by immunoblotting using proteinase K-treated samples could be detected by this PrP^{Sc}-specific immunofluorescence staining because of the omission of the protease treatment process. In the present study, we applied this method to frozen brain sections for the detection of PrP^{Sc} (Fig. 3C and D). Signals of PrP could be detected from the brains of prion-infected mice, but signals from the brains of uninfected mice remained at background levels under the same conditions (data not shown), demonstrating that this method can be applied to detect PrP^{Sc} from frozen brain sections. At 60 dpi, bright punctate staining of PrP^{Sc} was detected frequently in the thalamus and occasionally detected in the cerebral cortex of the WT mice infected with the Chandler strain. The PrP^{Sc} was also detected in parts of the thalamus of CD14$^{-/-}$ mice, but the occurrence was less frequent than in the same areas of WT mice (Fig. 3C and D). At 90 dpi, PrP^{Sc} was distributed more widely; PrP^{Sc} could be detected in the hippocampus as well as in the thalamus and cerebral cortex of WT and CD14$^{-/-}$ mice infected with the Chandler strain (Fig. 3D). However, the PrP^{Sc} staining in some brain areas of CD14$^{-/-}$ mice seemed to be still weaker than in the WT mice (Fig. 3C and D). There were no marked differences in the PrP^{Sc} distribution between the WT and CD14$^{-/-}$ mice at 120 dpi. Delay of the PrP^{Sc} accumulation was also observed in the brains of the Obihiro-infected CD14$^{-/-}$ mice. At 60 dpi, PrP^{Sc} was detected in the hippocampus and thalamus of WT mice but not in these areas of the CD14$^{-/-}$ mice. At 90 dpi, PrP^{Sc} was spread into the hypothalamus and amygdala of WT mice, but the presence of PrP^{Sc} in the CD14$^{-/-}$ mice was restricted to the hippocampus and thalamus.

We also analyzed the prion infectivity in the brains of WT and CD14$^{-/-}$ mice using Tga20 mice that overexpress mouse PrP and thus are highly susceptible to mouse-adapted prions (25). Prion infectivity in the brains of both of the Chandler-infected CD14$^{-/-}$ mice at 60 dpi was significantly lower than that in both of the WT mice (Fig. 4). Prion infectivity in the brains of the Obihiro-infected mice also appeared to be lower than those from WT mice; the infectivity in the brain of one CD14$^{-/-}$ mouse (no. 2) was significantly lower than that of one WT mouse (no.1). However, in the later stages, there were no significant differences in the prion infectivity of WT and CD14$^{-/-}$ mice in the Chandler or Obihiro infection (Fig. 4).

We also performed a histopathological analysis of the brains of WT and CD14$^{-/-}$ mice infected with the Chandler strain (Fig. 5). At 90 dpi, slight vacuolar degeneration of neuropil and neurons was only occasionally observed in the thalamus of Chandler-infected WT and CD14$^{-/-}$ mice. Vacuolar degeneration was widely observed throughout the brains after 120 dpi; however, there was no apparent difference in the severity and distribution of vacuolar degeneration of the WT and CD14$^{-/-}$ mice infected with the Chandler strain.

Microglial activation. Depletion of CD14 in a mouse model of Alzheimer's disease (AD) was reported to result in a reduction in the number of microglia (17). To assess if depletion of CD14 altered microglial activation in prion diseases, we analyzed the expression of an activated microglial marker, Iba1, by immunohistochemistry (Fig. 6). At 60 dpi, some microglia of CD14$^{-/-}$ mice had more protrusions than those of WT mice. Morphological differences in Iba1-positive microglia became more prominent at 90 dpi; microglia in CD14$^{-/-}$ mice had a larger cytoplasm and more branched protrusions than those of WT mice. At 120 dpi, Iba1-positive microglia in WT mice had a smaller cytoplasm and fewer protrusions; however, microglia in CD14$^{-/-}$ mice still had relatively larger cytoplasm with many protrusions. In the terminal stage, there were no obvious differences in the morphology of microglia of WT and CD14$^{-/-}$ mice.

The quantitative analysis of Iba1-positive microglia showed that in the hippocampus and thalamus of the Chandler-infected WT and CD14$^{-/-}$ mice the numbers of microglia increased from 60 to 120 dpi and then showed no further change or slightly decreased (Fig. 6B). Similar changes were observed in the Obihiro-infected WT and CD14$^{-/-}$ mice. In the Chandler-infected mice, there was little difference in the numbers of Iba1-positive microglia between the WT and CD14$^{-/-}$ mice by 90 dpi. At 120 dpi, Iba1-positive microglia increased more in the thalamus of CD14$^{-/-}$ mice than in WT mice. In the terminal stage, numbers of the Iba1-positive microglia decreased both in WT and

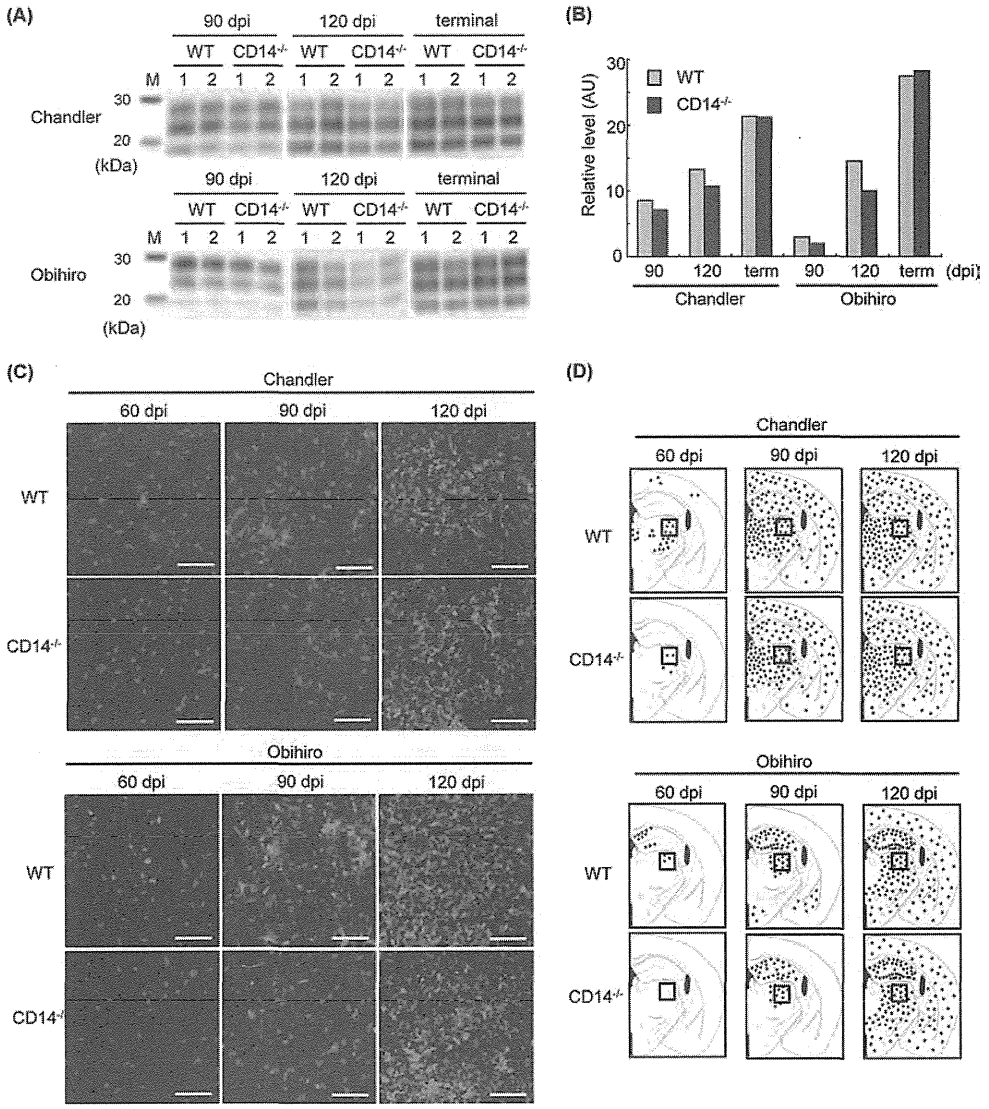

FIG 3 PrP^{Sc} accumulation in the brains of prion-infected WT and $CD14^{-/-}$ mice. (A) Detection of PrP-res by immunoblotting. Brains were harvested at 90 and 120 dpi and at the terminal stage. Brain tissue equivalents loaded were 500, 350, and 250 μg for the 90 and 120 dpi time points and the terminal stage of the disease, respectively. Two mice were used in each group. M, molecular mass marker. (B) Quantitative analysis of PrP-res. The results of immunoblotting were quantified using Multi Gauge ver 3.0 (Fuji Film). Each blot used 10 ng of rMoPrP for the normalization of the transfer efficiency, and the graphs show relative values (arbitrary units [AU]) to rMoPrP (average of the results from 2 mice). term, terminal stage of the disease. (C) Immunofluorescence staining of PrP^{Sc}. Frozen sections were prepared from the brains of WT and $CD14^{-/-}$ mice harvested at 60, 90, and 120 dpi and subjected to PrP^{Sc}-specific staining with MAb 132. Representative images from the thalamus are shown (representing the regions of the boxed areas in the corresponding images in panel D). Bars, 50 μm. Green, PrP^{Sc}. Blue, nuclei. (D) Summary of PrP^{Sc} distribution detected by PrP^{Sc}-specific staining.

$CD14^{-/-}$ mice, although those in the thalamus of $CD14^{-/-}$ mice were still slightly larger than those of WT mice. In the Obihiro-infected mice, there were no differences in the numbers of Iba1-positive microglia of the WT and $CD14^{-/-}$ mice at 60 dpi. At 90 and 120 dpi, numbers of Iba1-positive microglia in the thalamus of $CD14^{-/-}$ mice appeared to be larger than in the thalamus of WT mice. In the terminal stage, there were no marked differences in the numbers of Iba1-positive microglia of WT and $CD14^{-/-}$ mice.

To further characterize the differences in microglial activation of prion-infected WT and $CD14^{-/-}$ mice, we performed immunofluorescence staining for other microglial markers (Fig. 7). Expression of CD11b, a commonly used microglial marker, was elevated in the brains of WT and $CD14^{-/-}$ mice from 90 to 120 dpi, and the expression of CD11b in $CD14^{-/-}$ mice was more intense than that in WT mice at each time point. A marker for macrophages and monocytes, F4/80, is also frequently used as a microglial marker. Similar to CD11b, F4/80 immunoreactivity was detected more in $CD14^{-/-}$ mice than in WT mice at 90 and 120 dpi. Similar changes were also observed in the immunofluorescence staining for CD68, a phagocytic marker of macrophages and microglia: CD68-positive cells increased time dependently both in

(A) Chandler

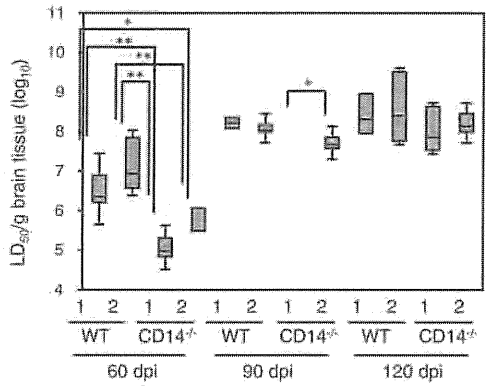

(B) Obihiro

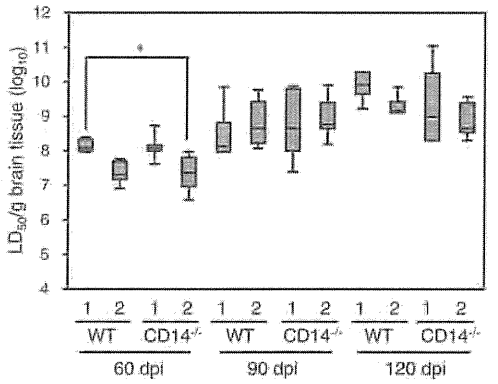

(C) Chandler

Inoculum	Mouse No.	Survival time (days)	Mean ± SD (days)
WT, 60 dpi	1	65, 68, 69, 70, 72	68.7 ± 2.6
	2	63, 64, 64, 67, 67, 70, 70	66.4 ± 2.9
CD14$^{-/-}$, 60 dpi	1	75, 78, 79, 81	78.3 ± 2.5
	2	71, 71, 75, 75, 75	73.4 ± 2.2
WT, 90 dpi	1	60, 60, 60, 63	60.8 ± 1.5
	2	59, 61, 61, 62	60.8 ± 1.3
CD14$^{-/-}$, 90 dpi	1	59, 59, 59, 60	59.2 ± 0.4
	2	61, 63, 63, 65	63.0 ± 1.6
WT, 120 dpi	1	58, 58, 61, 63	60.0 ± 2.4
	2	56, 56, 57, 59, 60, 65, 68	59.3 ± 4.5
CD14$^{-/-}$, 120 dpi	1	59, 59, 61, 63, 64, 66	62.0 ± 2.8
	2	58, 60, 61, 62	60.2 ± 1.7

(D) Obihiro

Inoculum	Mouse No.	Survival time (days)	Mean ± SD (days)
WT, 60 dpi	1	98, 98, 100, 100, 101, 101	99.7 ± 1.4
	2	88, 104, 111, 113, 115, 119	108.3 ± 11.1
CD14$^{-/-}$, 60 dpi	1	95, 100, 100, 100, 101, 104	100.0 ± 2.9
	2	107, 109, 111, 111, 111, 125, 125	114.1 ± 8.1
WT, 90 dpi	1	86, 89, 101, 101	96.5 ± 7.1
	2	89, 91, 95, 95, 100, 100	95.0 ± 4.5
CD14$^{-/-}$, 90 dpi	1	90, 91, 99, 106	96.5 ± 7.5
	2	85, 88, 91, 94, 94, 96	92.4 ± 4.8
WT, 120 dpi	1	83, 83, 85, 90	85.3 ± 3.3
	2	85, 90, 91, 91	89.3 ± 2.8
CD14$^{-/-}$, 120 dpi	1	80, 87, 92, 98, 98	91.0 ± 7.7
	2	88, 90, 95, 96, 98	93.4 ± 4.2

FIG 4 Prion infectivity. (A, B) Prion infectivity in the brains of WT and CD14$^{-/-}$ mice infected by the Chandler (A) or Obihiro (B) strain. The infectivity was measured by bioassay using Tga 20 mice. *, $P < 0.05$; **, $P < 0.001$ (analysis of variance [ANOVA] followed by Dunnett's *post hoc* test). (C, D) Survival times of Tga 20 mice used for bioassay. Survival time for each Tga 20 mouse inoculated with brain homogenates from the Chandler-infected (C) or Obihiro-infected (D) WT or CD14$^{-/-}$ mice is shown. The difference in the Chandler-infected CD14$^{-/-}$ mice at 90 dpi was due to the small standard deviation of mouse no. 1: three of four Tga20 mice in this group reached the terminal stage on the same day.

WT and in CD14$^{-/-}$ mice, and CD68 immunoreactivity was more prominent in CD14$^{-/-}$ mice than in WT mice. We also analyzed CD45, a common leukocyte antigen expressed on all leukocytes. Ramified parenchymal microglia express lower levels of CD45 than peripheral macrophages (26, 27), while the expression of CD45 in microglia may be increased under certain pathological conditions such as HIV encephalitis (28, 29) and Alzheimer's disease (30). For the study here, expression of CD45 was clearly more upregulated in CD14$^{-/-}$ mice than in WT mice at 90 and 120 dpi (Fig. 7).

Expression of anti-inflammatory cytokines. Depletion of CD14 in the AD model mouse resulted in a reduced amyloid β (Aβ) plaque burden with the increased gene expression of the anti-inflammatory cytokine IL-10 (17). Similar to the reduced Aβ plaque burden in AD model mice lacking CD14$^{-/-}$, this study observed that accumulation of PrP^{Sc} in prion-infected CD14$^{-/-}$ mice was delayed by 90 dpi (Fig. 3C and D). The knockout of the *IL-10* gene has been shown to greatly shorten the survival time of prion-infected mice, suggesting a protective role of IL-10 in the progression of prion diseases (8). Therefore, we analyzed the anti-inflammatory cytokine expression in prion-infected CD14$^{-/-}$ mice to determine if a lack of CD14 modulates the inflammatory response in the brain.

Compared to the mock-infected mice, the prion-infected WT mice showed a weak but detectable IL-10 expression from 60 to 120 dpi. Interestingly, IL-10 immunoreactivity was observed more frequently in the thalamus of CD14$^{-/-}$ mice than in WT mice throughout the time of observation (Fig. 8A), and IL-10 immunoreactivity in CD14$^{-/-}$ mice appeared to increase from 60 to 90 dpi but to decrease from 90 to 120 dpi. The IL-10-positive areas were quantified and statistically analyzed if more than 3 mice were available. At 60 dpi, the areas positive for IL-10 in CD14$^{-/-}$ mice were significantly larger than in WT mice ($P < 0.01$, Student's *t* test) (Fig. 8B). The IL-10-positive areas in CD14$^{-/-}$ mice were also larger than those in WT mice at 90 and 120 dpi. We also examined the cell type in the brains expressing IL-10 by double staining (Fig. 8C to F). Most of the IL-10 immunoreactivity was detected in CD11b- or Iba1-positive microglia (Fig. 8C and D) and some in NeuN-positive neurons (Fig. 8E), in the brains of both WT and CD14$^{-/-}$ mice from 60 to 120 dpi. There was no IL-10 immunoreactivity detected in GFAP-positive astrocytes (Fig. 8F).

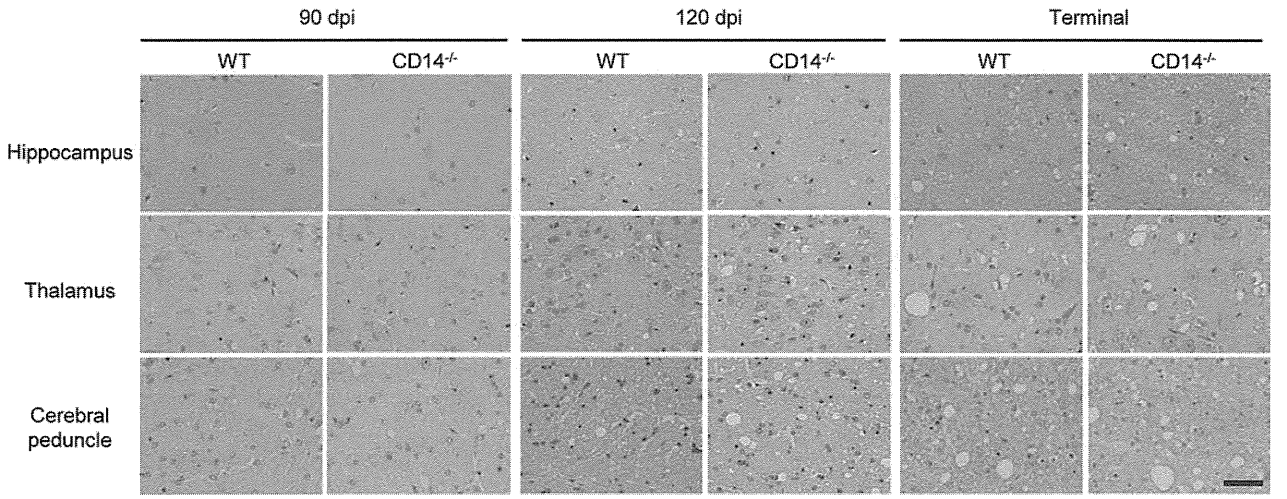

FIG 5 Histopathological analysis of the brains of prion-infected WT and CD14$^{-/-}$ mice. Representative images from the thalamus, the hippocampus, and the cerebral peduncle of the Chandler-infected mice are shown. Bar, 50 μm.

We also analyzed another anti-inflammatory cytokine, TGF-β (Fig. 9A), which has been reported to play a role in the suppression of progression of prion diseases (9). At 60 dpi, TGF-β immunoreactivity was observed more frequently in CD14$^{-/-}$ mice than in WT mice infected with the Chandler or Obihiro strains. Although no significant difference was observed in TGF-β-positive areas between WT and CD14$^{-/-}$ mice at 60 dpi ($P = 0.053$, Student's t test), the areas in two of three samples from the CD14$^{-/-}$ mice were larger than in all samples from WT mice (Fig. 9B), suggesting this tendency. However, little difference in the TGF-β immunoreactivity was observed between WT and CD14$^{-/-}$ mice after 90 dpi (Fig. 9A and B). However, there was little difference in the TGF-β immunoreactivity of WT and CD14$^{-/-}$ mice after 90 dpi. Double staining showed that TGF-β immunoreactivity was detected mostly in CD11b- and Iba1-positive microglia (Fig. 9C and D) and only occasionally in NeuN-positive neurons (Fig. 9E). Very little TGF-β immunoreactivity was detected in GFAP-positive astrocytes (Fig. 9F).

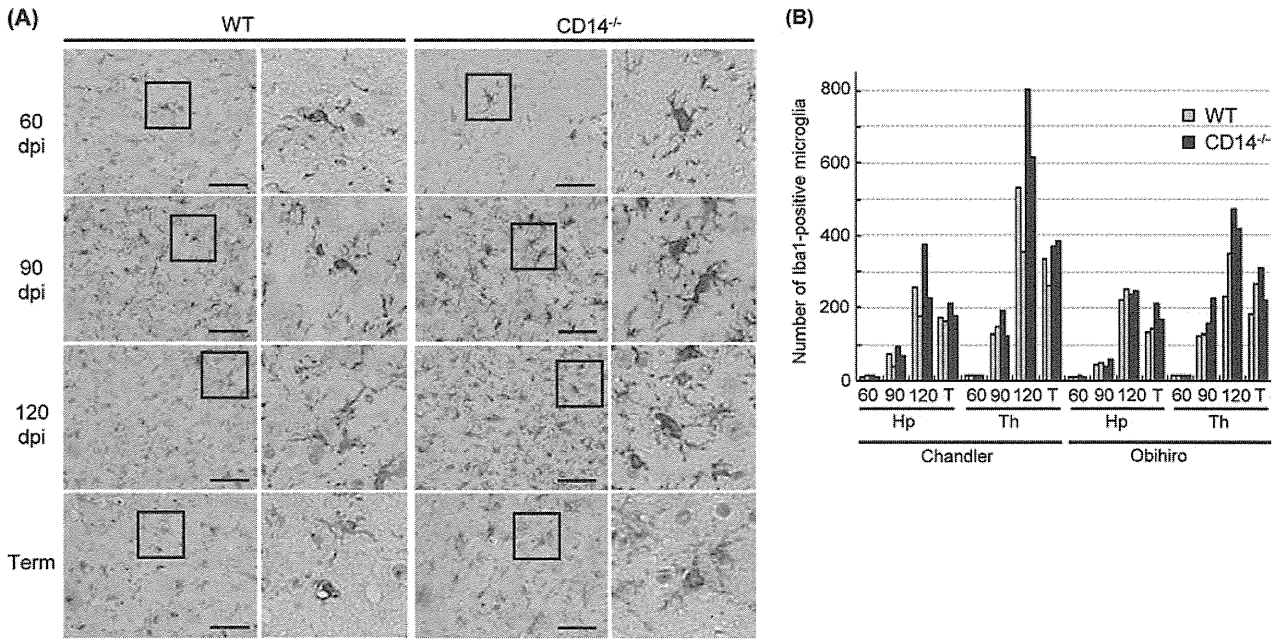

FIG 6 Expression of an activated microglial marker, Iba1, in the brains of prion-infected WT and CD14$^{-/-}$ mice. (A) Immunohistochemistry for Iba1. Representative images from the thalamus of the Chandler-infected mice are shown. Higher magnifications of the areas indicated by boxes are shown in the corresponding right panels. Bars, 20 μm. Term, terminal stage. (B) Quantitative analysis of Iba1-positive microglia. Numbers of Iba1-positive cells in the hippocampus and the thalamus (1.5×10^{-1} mm^2 tissue section) were determined by Image J. Data are for 2 mice from each group. T, terminal stage; Hp, hippocampus; Th, thalamus.

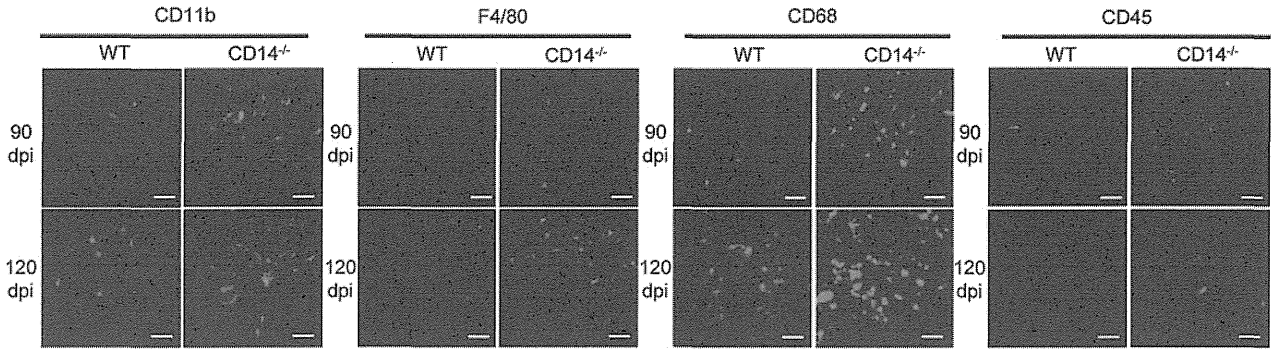

FIG 7 Immunofluorescence staining for microglial markers in the brains of prion-infected WT and CD14$^{-/-}$ mice. Frozen blocks of the brains harvested at 90 and 120 dpi were subjected to immunofluorescence staining for microglial markers CD11b, F4/80, CD68, and CD45. Representative images from the thalamus of the Chandler-infected mice are shown. Bars, 50 μm.

Expression of proinflammatory cytokine. We also assessed if a lack of CD14 influenced the expression of proinflammatory cytokines in the brains of prion-infected mice. Here, we focused on IL-1β, since a lack of IL-1β receptor signaling has been reported to delay the progression of prion diseases (7). Different from the situation in anti-inflammatory cytokines, more immunoreactivity of IL-1β was detected in WT mice than in CD14$^{-/-}$ mice at 60 and 90 dpi, particularly in the corpus callosum, internal capsules, and cerebral peduncles (Fig. 10A). Quantitative analysis showed that IL-1β-positive areas in the internal capsule of WT mice were significantly larger than the same areas of CD14$^{-/-}$ mice at 60 dpi ($P < 0.05$, Welch's t test) (Fig. 10B). Also, IL-1β-positive areas of WT mice tended to be larger than those of CD14$^{-/-}$ mice at 90 and 120 dpi (Fig. 10B), although statistical analyses could not be carried out due to the limited number of animals ($n = 2$). The differences in the expression of IL-1β of WT and CD14$^{-/-}$ mice appeared to be less prominent in the thalamus throughout the time of the observations (data not shown).

DISCUSSION

Prolonged survival of prion-infected CD14$^{-/-}$ mice and delayed PrP^{Sc} deposition in the brains suggest that CD14 plays a role in acceleration of disease progression after prion infection. Similarly, depletion of CD14 reduced Aβ deposition in a mouse model of AD (17), suggesting that CD14 could also play a role in other neurodegenerative disorders. However, microglial activation is different in prion-infected and AD model mice lacking CD14; microglia in CD14$^{-/-}$ mice infected with prions were more strongly activated than in WT mice, particularly in the early stage of the disease, whereas there is reduced microglial activation in AD model mice lacking CD14 (17).

There is a line of evidence that microglial activation causes detrimental effects in prion diseases. For instance, there is a report that a blockade of the colony-stimulating factor 1 receptor (CSF1R) signaling pathway reduced microglial proliferation in the brains of prion-infected mice and slowed the disease progression (31). Prion-infected mice deficient for CD40 ligand showed shortened incubation periods with increased microglial activation (32). Furthermore, prion-infected CXCR3-deficient mice survived longer than WT mice with reduced microglial activation, although prion propagation and PrP^{Sc} accumulation were accelerated (33). Here, in contrast, we showed that microglia were more activated in prion-infected CD14$^{-/-}$ mice than in WT mice but that prion-infected CD14$^{-/-}$ mice survived longer than WT mice. This result implies that microglial activation in the CD14$^{-/-}$ mice could offer a protective effect in the disease progression after prion infection. Particularly, the relationship between the increased microglial activation and delayed PrP^{Sc} accumulation in CD14$^{-/-}$ mice is intriguing. Priller et al. reported that during the course of prion infection, first the resident microglia were activated and thereafter bone marrow-derived microglia colonized the brain of the prion-infected mice, and more than 50% of the microglia were replaced by bone marrow-derived microglia by the onset of the disease (34). Thus, it is possible that the origin and activation state of microglia differ in the early and in the late stages of prion diseases. Here, we showed that the increased activation of microglia in prion-infected CD14$^{-/-}$ is concomitant with the upregulation of the anti-inflammatory cytokine production such as IL-10 and the delayed PrP^{Sc} accumulation. The precise phenotype of the microglia at this time point remains to be elucidated, but it is suggested that microglia activated in the early stage of prion infection in the CD14$^{-/-}$ mice possess a neuroprotective potential.

Although an accelerating role of CD14 in the progression of prion diseases is suggested by the current study, the mechanism by which CD14 works in the process of the disease needs to be further elucidated. One possible involvement of CD14 indicated by the results of the immunofluorescence staining for anti-inflammatory cytokines is that it downregulates alternative activation of microglia directly or indirectly. Induction of a proinflammatory response is another possible function of CD14 in prion diseases. CD14 is a GPI-anchoring protein and thus lacks an intracellular domain, but it works together with the TLR4 homodimer to induce cellular signaling involved in proinflammatory responses (12). Therefore, a lack of CD14 affects the signaling through the CD14/TLR4 complex, which could be a cause of the longer survival of prion-infected CD14$^{-/-}$ mice. However, a previous study showed that TLR4-signaling mutant mice, C3H/HeJ (*Tlr4*$^{Lps\text{-}d}$) mice, possessing a single amino acid mutation in the cytoplasmic domain, were highly susceptible to prion infection, suggesting that TLR4 signaling can interfere with the disease progression (35). This is seemingly contradictory to the results of our study here. However, TLR4 is not the only counterpart of CD14: CD14 is reported to form clusters with a TLR2-TLR6 heterodimer (36).